Development 134, 1809-1817 (2007) doi:10.1242/dev.02843

The Mrj co-chaperone mediates keratin turnover and prevents the formation of toxic inclusion bodies in trophoblast cells of the placenta

Erica D. Watson, Colleen Geary-Joo, Martha Hughes and James C. Cross*

Defects in protein-folding and -degradation machinery have been identified as a major cause of intracellular protein aggregation and of aggregation-associated diseases. In general, it remains unclear how these aggregates are harmful to normal cellular function. We demonstrate here that, in the developing placenta of the mouse, the absence of the Mrj (Dnajb6) co-chaperone prevents proteasome degradation of keratin 18 (K18; Krt18) intermediate filaments, resulting in the formation of keratin inclusion bodies. These inclusions in chorionic trophoblast cells prevent chorioallantoic attachment during placental development. We show further that keratin-deficient embryos undergo chorioallantoic attachment and that, by genetically reducing keratin expression in $Mrj^{-/-}$ conceptuses, chorioallantoic attachment was rescued. Therefore, the chorioallantoic attachment phenotype in *Mrj* mutants is not due to a deficiency of the normal keratin cytoskeleton, but rather is cytotoxicity caused by keratin aggregates that disrupt chorion trophoblast cell organization and function.

KEY WORDS: Mrj, Keratin, Aggregation, Hsp40 co-chaperone, Proteasome, Chorioallantoic attachment, Tetraploid aggregation, Placenta, Mouse

INTRODUCTION

Protein aggregation and the formation of intracellular protein inclusion bodies are associated with many degenerative disorders, including Parkinson's and Huntington's diseases, and with cirrhosis of the liver (Carrell, 2005). In many cases, the role of protein aggregates in disease pathogenesis is unclear. Efforts to understand aggregation disorders have focused mainly on mutations within the disease-associated protein. However, mounting evidence suggests that a major cause of protein inclusion body formation is failure of the protein quality-control system (McClellan et al., 2005). This surveillance mechanism recruits both molecular chaperones and proteases to safeguard against protein aggregation by maintaining the equilibrium between protein folding and degradation (Hohfeld et al., 2001).

A malfunction in the ubiquitin-proteasome degradation pathway is hypothesized to be one cause of Mallory body formation in the hepatocytes of patients with chronic liver disorders (Bardag-Gorce et al., 2003; Bardag-Gorce et al., 2004; Denk et al., 2000). Mallory bodies are inclusions composed of the keratin intermediate filaments keratin 8 (K8; also known as Krt8) and keratin 18 (K18; also known as Krt18), as well as ubiquitin, the proteasome complex and molecular chaperones, including heat shock protein 70 (HSP70; HSPA1B) and heat shock protein 90 (HSP90) (Coulombe and Omary, 2002). Cells that have been treated with a chemical inhibitor of proteasome function (Bardag-Gorce et al., 2004) or that contain the UBB^{+1} ubiquitin mutation (Bardag-Gorce et al., 2003) form Mallory bodies due to an accumulation of non-degraded keratin.

Misfolded proteins also tend to aggregate. Proper protein folding within a cell often does not occur spontaneously and, thus, molecular chaperones are required for some proteins to reach its native state efficiently (Hartl and Hayer-Hartl, 2002). Hsp70 is a ubiquitous chaperone that, together with diverse co-chaperone binding partners, facilitates protein folding and the presentation of proteins to the proteasome for degradation (Esser et al., 2004). Co-chaperones of the DnaJ (Hsp40) protein family are characterized by a conserved J-domain that regulates substrate binding and release by activating the ATPase activity of Hsp70 (Fan et al., 2003). These co-chaperones differ in their tissue and subcellular patterns of expression, and convey substrate specificity to Hsp70 (Fan et al., 2003). However, little is known about the precise substrates that are regulated in this manner.

The *Mrj* (Mammalian relative of DnaJ; also known as *Dnajb6* – Mouse Genome Informatics) gene encodes a co-chaperone that is widely expressed throughout the adult mouse and during development of the embryo and placenta (Chuang et al., 2002; Dai et al., 2005; Hunter et al., 1999; Izawa et al., 2000; Seki et al., 1999). $Mrj^{-/-}$ embryos die at mid-gestation due to a failure of chorioallantoic attachment during placental development (Hunter et al., 1999). Recently, a few diverse Mrj-interacting proteins have been identified, including Huntington disease (HD) protein (Chuang et al., 2002) and K18 (Izawa et al., 2000). Here, we show that *Mrj* deficiency prevents normal keratin turnover, resulting in the formation of large keratin aggregates that are toxic to trophoblast cells, inhibiting their normal function.

MATERIALS AND METHODS

Mice

$Mrj^{+/-}$ mice were originally generated by *6AD1 β-geo* gene-trap insertion as previously described (Hunter et al., 1999). $Mrj^{-/-}$ embryos were produced by mating $Mrj^{+/-}$ mice. *K18*/*K19* double-null embryos were generated by mating $K18^{-/-}$ mice (Magin et al., 1998) with $K19^{-/-}$ mice (Hesse et al., 2000) (provided by T. Magin, University of Bonn, Bonn, Germany) and then mating the resulting double heterozygous progeny. $Mrj^{-/-}$;$K18^{-/-}$ and $Mrj^{-/-}$;$K18^{+/-}$ embryos were generated by mating $Mrj^{+/-}$ mice with $K18^{-/-}$ mice and then mating their resulting $Mrj^{+/-}$;$K18^{+/-}$ progeny together. Enhanced green fluorescent protein (*Egfp*) transgenic mice (Hadjantonakis et al., 1998) were maintained at heterozygosity in a

Department of Biochemistry and Molecular Biology, University of Calgary, Calgary, Alberta, T2N 4N1, Canada.

*Author for correspondence (e-mail: jcross@ucalgary.ca)

Accepted 26 February 2007

CD-1 background. Experiments were performed in accordance with the Canadian Counsel on Animal Care and the University of Calgary Committee on Animal Care (Protocol no. M01025).

Genotyping

Mrj genotypes were determined by PCR using primers 5′-CCA-ATAGCAGCCAGTCCCTTCCC-3′ and 5′-TTCGGCTATGACTGGGC-ACAACA-3′ to detect the neomycin-resistance gene of the *β-geo* cassette (226 bp, mutant allele); and 5′-ACAGGGTCTTGCTACAAGTAGTGC-3′ and 5′-TTTCTCTGTCCATGAAGGACTGGG-3′ to detect the *β-geo* gene-trap insertion site in *Mrj* intron 2 (463bp, wild-type allele). The PCR parameters were 30 seconds at 94°C, 30 seconds at 63°C and 30 seconds at 72°C for 30 cycles. Genotyping for *K18* and *K19* (*Krt19*) mice was performed as previously described (Hesse et al., 2000; Magin et al., 1998).

Generation of tetraploid aggregation chimeras

Tetraploid aggregation chimeras were generated as described previously (Nagy et al., 2003). Briefly, tetraploid embryos were formed by electrofusing two-cell *Egfp* embryos, which were then aggregated with eight-cell diploid embryos from *Mrj* heterozygous matings. Aggregated chimeric embryos were allowed to develop to the blastocyst stage and were then transferred into the uteri of pseudopregnant CD-1 females [noon of the day that the vaginal plug is detected was defined as embryonic day (E)0.5]. Embryos were dissected at E9.5. The existence of wild-type tetraploid cells within the placenta was determined by the presence or absence of enhanced GFP (EGFP) expression using a GFP filter (41017 EN GFP, Leica). The yolk sac and embryo tissue was removed for *Mrj* genotyping. Placentas were fixed in 4% paraformaldehyde (PFA; VWR) in 1× phosphate buffered saline (PBS) and embedded in paraffin. Tissue sections were stained with hematoxylin and Eosin (both Sigma).

Cell cultures

Wild-type (line 6-3) and *Mrj* homozygous mutant (lines 1-4 and 4-1) trophoblast stem (TS) cell lines were derived from littermate blastocysts generated from *Mrj* heterozygote matings. Blastocysts were allowed to outgrow on embryonic feeder cells in TS cell medium (Tanaka et al., 1998). These TS cell lines and the *Rs26* TS cell line (provided by J. Rossant, Hospital for Sick Children, Toronto, Canada) (Tanaka et al., 1998) were maintained in 25 ng/ml basic fibroblast growth factor (bFGF), 1 μg/ml heparin in TS cell medium, 70% of which was pre-conditioned by embryonic fibroblasts, at 37°C under 95% humidity and 5% CO_2. Cells were differentiated by withdrawing bFGF, heparin and fibroblast-conditioned medium (Tanaka et al., 1998).

Chorion-ectoplacental cones were dissected at E7.5 from *Mrj* heterozygous crosses in 1× PBS. Explants were placed in 0.125% trypsin/EDTA (Gibco) in PBS for 10 minutes at 37°C. Dispersed cells were then cultured on coverslips in fibroblast-conditioned TS cell medium with bFGF and heparin for 5 days at 37°C in 95% humidity, 5% CO_2, with daily medium change. Yolk sacs were removed during dissection for genotyping.

X-gal and immunofluorescence antibody staining

Mouse conceptuses were dissected at E8.25 and E9.5. For X-gal staining, tissue was fixed, stained as whole mount and was then paraffin embedded as previously described (Hunter et al., 1999). For antibody staining, tissue was fixed in 4% PFA and embedded in paraffin. Paraffin sections (7 μm) were rehydrated in ethanol, treated with trypsin tablets (Sigma) in PBS for 10 minutes and blocked in 1% bovine albumin serum (BSA; Sigma), 5% host serum for 1 hour. Cell cultures were fixed in 4% PFA for 10 minutes, treated with 0.1% Triton X-100 (Fisher Biotech) for 10 minutes and blocked in 1% BSA for 30 minutes. Primary antibodies and dilutions used include: anti-cytokeratin 18 (Ks18.04, 1:100; RDI), anti-keratin 8 (Ks8.7, 1:100; Progen), anti-keratin 19 (Troma.3, 1:100; a gift from T. Magin), anti-pan-cytokeratin (1:100; DAKO), anti-desmoplakin (DP1&2, neat; RDI), anti-20S proteasome core subunits (1:100; Calbiochem) and anti-Mrj (020417, 1:100; a gift from M. Inagaki, Aichi Cancer Centre Research Institute, Aichi, Japan) (Izawa et al., 2000). Secondary antibodies were used at a dilution of 1:300 and included: goat anti-rabbit Cy3, goat anti-rat Cy3, goat anti-mouse Cy3 and goat anti-rabbit FITC (Jackson ImmunoResearch Laboratories), and goat anti-mouse Alexa Fluor 488 (Molecular Probes). Antibody dilutions were made in 1% BSA, 5% host serum. DNA was counterstained with 1:10,000 bisbenzimide (Sigma).

Electron microscopy

E8.25 implantation sites from *Mrj* heterozygous matings were fixed in 2% EM-grade glutaraldehyde (Sigma), 2% PFA in 0.2 M sodium cacodylate (pH 7.4; Sigma) overnight at 4°C, and were post-fixed in 1% osmium tetroxide (EM Sciences) in 0.2 M sodium cacodylate (pH 7.4) for 2 hours at 4°C. Tissue was dehydrated in increasing concentrations of ethanol up to 70%, treated in 2% uranyl acetate (ProSciTech) in 70% ethanol, and further dehydrated in increasing ethanol concentrations (70-100%). Tissue was treated with propylene oxide (EM Sciences) and was resin embedded (EMBED 812 kit, EM Sciences). Yolk sacs were removed for genotyping prior to fixation.

Proteasome inhibition assay

Rs26 TS cells were differentiated by withdrawal of bFGF, heparin and fibroblast-conditioned media for 4 days on coverslips. Cells were exposed to 10 μM clasto-lactacystin β-lactone (Invitrogen) in differentiating TS medium overnight at 37°C under 95% humidity and 5% CO_2. Cells were washed with 1×PBS, fixed in 4% PFA and immunostained as described above.

Equipment and software

A Leica DMR light microscope (for fluorescent and light images), Leica DMIL inverted light microscope (for cell culture images) and Leica MZ95 dissection microscope (for dissected embryo/placenta images) with Photometrics Coolsnap cf camera and Open Lab 2.2.2 imaging software program were used to obtain micrographs. Filters used were from Chroma: DAPI (31000), TRITC (31002) and FITC (31001). De-convolved images were captured using an Axioplan 2 Imaging (Zeiss) microscope and Axiovision 4.1 acquisition software. Electron micrographs were taken on a Hitachi 7000 transmission electron microscope. Minimal image processing was performed using Adobe Photoshop 7.0 and figures were constructed using Canvas X.

RESULTS

Mrj-deficient embryos fail to undergo chorioallantoic attachment because of defects within chorionic trophoblast cells

The chorion layer of the mouse placenta is composed of two cell types at embryonic day (E)7.5: chorionic trophoblast cells and a thin inner layer of extra-embryonic mesothelium. Normally, chorioallantoic attachment begins at approximately E8.0 when the allantois, composed of extra-embryonic mesoderm, grows from the posterior end of the embryo across the exocoelomic cavity to first contact and then firmly attach to the chorionic mesothelium (Downs, 2002). Stable attachment is required for allantoic spreading along the surface of the chorion and for the formation of trophoblastic villi (reviewed by Watson and Cross, 2005). *Mrj* mutant conceptuses fail to undergo chorioallantoic attachment and as a result do not form a mature placenta, dying by E10.5 (Hunter et al., 1999). *Mrj* mutant allantoises appear to both expand and elongate normally compared to wild type at E8.0 (Hunter et al., 1999), and grow across the exocoelomic cavity to contact the chorion. However, despite the close proximity of the allantois to the chorion, subsequent firm attachment to the chorion is not observed. Our initial observations have been confirmed in careful dissections of conceptuses after E8.5, showing the inability of the allantois to stay attached to the chorion in all mutants (n=81). Presumably as a consequence of failing to attach the chorion, the allantois rapidly collapsed and shrunk back to form a bud of tissue at the posterior end of the embryo by E9.5 (see Fig. S1 in the supplementary material). This phenomenon has been observed in

other mutants with defects in chorioallantoic attachment (Hildebrand and Soriano, 2002; Tetzlaff et al., 2004; Yang et al., 1995).

Failure of chorioallantoic attachment in the *Mrj* mutants was presumably due to a chorionic cell defect, because *Mrj* expression has been detected within the chorion and not the allantois (Hunter et al., 1999). Using β-galactosidase activity driven from the *Mrj* gene-trap allele (Fig. 1A) and Mrj antibody staining (Fig. 1B) on E8.25 histological sections, we detected Mrj expression throughout the chorionic trophoblast. However, expression within the chorionic mesothelium was indeterminable because of the thinness of this cell layer.

To address better whether Mrj is required within the chorionic trophoblast and/or the mesothelium for chorioallantoic attachment, we used tetraploid aggregation, a technique that has previously been shown to produce chimeric conceptuses with genetically distinct chorionic cell compartments (Fig. 1C) (Tarkowski et al., 1977). Wild-type tetraploid embryos were aggregated with diploid embryos derived from *Mrj* heterozygous matings. The resulting conceptuses developed so that the chorionic mesothelium, embryo proper and allantois were almost exclusively composed of diploid cells (Tarkowski et al., 1977). By contrast, wild-type tetraploid cells contributed to the trophoblast lineage, resulting in a chorionic trophoblast layer that contains wild-type cells (Tarkowski et al., 1977). Therefore, we expected that, if Mrj is required only within chorionic trophoblast cells, and not in the mesothelium or allantois, then chorioallantoic attachment would be rescued in *Egfp⇔Mrj*$^{-/-}$ (tetraploid⇔diploid) chimeric conceptuses.

Chimeric blastocysts (n=24) were transferred into the uteri of pseudopregnant female mice. At E9.5, 1 day after chorioallantoic attachment is normally complete, all 15 surviving chimeric embryos had undergone chorioallantoic attachment. Genotyping revealed that two of these embryos were *Mrj* mutants (Fig. 1D,E), indicating that Mrj is not required within the mesothelium or allantois for chorioallantoic attachment to occur. Furthermore, development proceeded normally up to E9.5 in *Egfp⇔Mrj*$^{-/-}$ chimeric placentas, as indicated by the initiation of branching morphogenesis (Fig. 1H), similar to *Egfp⇔Mrj*$^{+/+}$ and *Egfp⇔Mrj*$^{+/-}$ littermates (Fig. 1F and data not shown). This is in contrast to *Mrj*-deficient chorions, which remained flat (Fig. 1G). These data imply that Mrj function was required exclusively within the trophoblast compartment at the chorioallantoic interface.

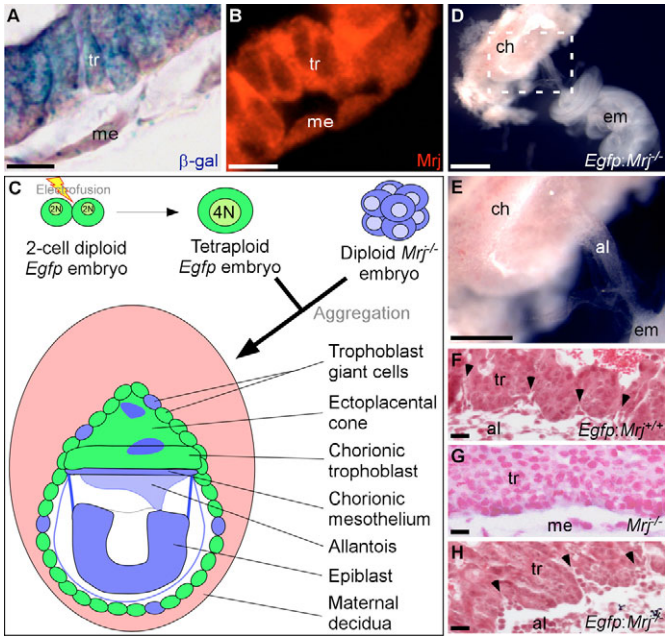

Fig. 1. *Mrj*$^{-/-}$ embryos fail to undergo chorioallantoic attachment because of defects within the chorionic trophoblast layer. (**A**,**B**) Expression of the β-galactosidase (β-gal; A; blue) and Mrj (B; red) proteins in E8.25 chorions. (**C**) Aggregation of a diploid *Mrj*$^{-/-}$ embryo (blue) with a wild-type tetraploid embryo expressing the *Egfp* transgene (green) results in a genetically mosaic chorionic trophoblast, ectoplacental cone and trophoblast giant cell layer (Rossant and Cross, 2001). The chorionic mesothelium, allantois and embryo proper are almost exclusively composed of *Mrj*-deficient diploid cells. (**D**,**E**) Rescued chorioallantoic attachment in an *Egfp:Mrj*$^{-/-}$ chimeric conceptus at E9.5. (E) Higher-magnification of boxed region in D. (**F-H**) Initiation of branching morphogenesis in the placental labyrinth layer (arrowheads) at E9.5 in *Egfp:Mrj*$^{+/+}$ (F) and *Egfp:Mrj*$^{-/-}$ (H) chimeric placentas, but not in a *Mrj*$^{-/-}$ chorion (G), which remains flat. al, allantois; ch, chorion; em, embryo; me, chorionic mesothelial layer; tr, chorionic trophoblast layer. Scale bars: 10 μm in A,B,F-H; 1 mm in D; 0.5 mm in E.

Mrj is required for a normal keratin cytoskeleton in trophoblast giant cells

Previous studies have demonstrated that Mrj binds to both soluble and filamentous K18 (Izawa et al., 2000). Because, in our study, Mrj function in the placenta was restricted to the trophoblast lineage, where keratin is also expressed, we explored whether *Mrj* mutant cells had a defective keratin cytoskeleton. Using immunofluorescence, we examined K18-containing filament organization within *Mrj*$^{-/-}$ trophoblast cells derived from primary cultures of explanted chorion-ectoplacental cone tissues. The chorionic trophoblast and ectoplacental cones are thought to be composed of multiple progenitor populations (Simmons and Cross, 2005), yet in culture they spontaneously differentiate primarily into trophoblast giant cells. Compared with 89.7% of wild-type trophoblast giant cells (n=659), only 36.9% of *Mrj*-deficient cells (n=634) had a normal, dense keratin filamentous network (Fig. 2A,B). Strikingly, the majority of *Mrj*$^{-/-}$ cells exhibited a collapsed keratin network, in which large perinuclear inclusions of keratin were present (53.9% compared with only 5.0% of wild-type cells). The remaining *Mrj*$^{-/-}$ cells contained either sparse keratin filaments (5.8%), or K18 levels were undetectable (3.4%).

All trophectoderm-derived cells express simple epithelial type I (K18 and K19) and type II (K7 and K8) keratins (Lu et al., 2005). Each keratin filament is composed of type I and type II heterodimers. K8 can dimerize with both K18 and K19 (Owens and Lane, 2003). Therefore, we also immunostained cells using K8, K19 and pan-cytokeratin antibodies. Interestingly, the results were similar to the collapsed K18 cytoskeleton or sparse K18 filaments observed (Fig. 2A,B). Ultrastructural analysis of keratin aggregates using electron microscopy in vivo revealed that they consisted of closely packed, parallel filaments (Fig. 2C). From this, we concluded that Mrj was required for the maintenance and/or turnover of the keratin cytoskeleton, but not for the assembly of filaments per se.

The keratin cytoskeleton appeared normal in approximately a third of *Mrj*-deficient trophoblast giant cells derived from explants (Fig. 2B). However, we noted that 37.4% of wild-type trophoblast giant cells (n=1478) had undetectable levels of Mrj at E8.25 (Fig. 2D), indicating that not all trophoblast giant cells would be expected

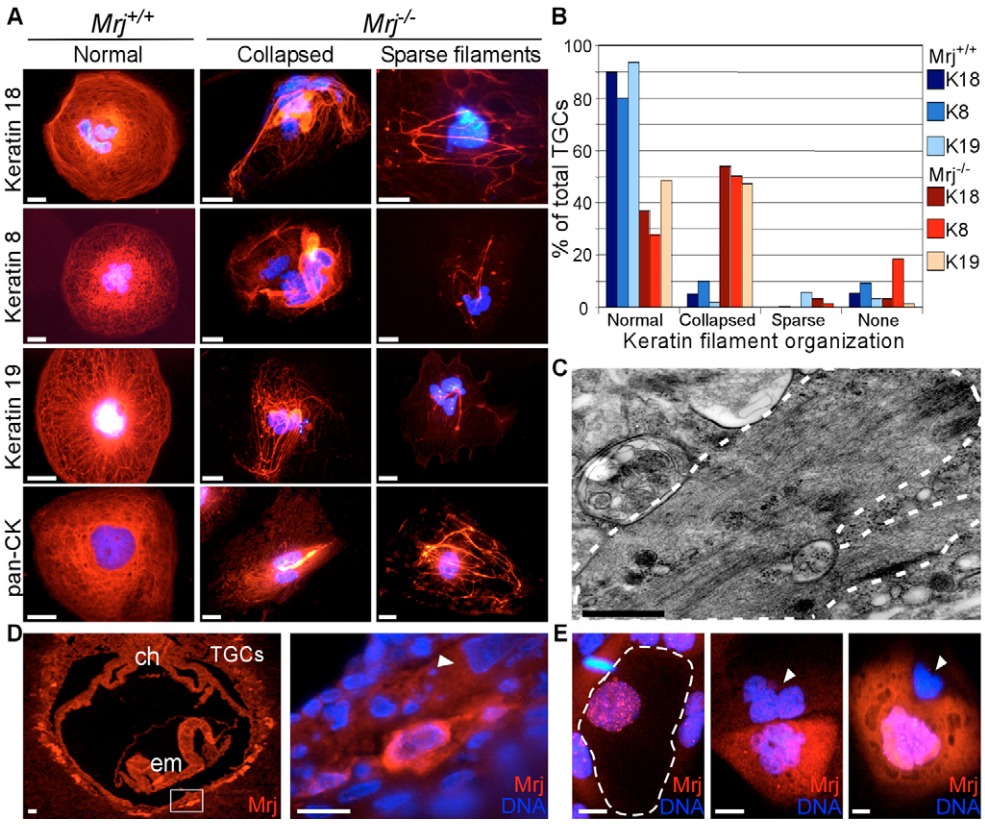

Fig. 2. The keratin cytoskeleton is collapsed in primary cultures of *Mrj*$^{-/-}$ trophoblast cells. (**A**) Keratin-filament (red) organization in trophoblast giant cells derived from wild-type and *Mrj*$^{-/-}$ chorion-ectoplacental cone explants. (**B**) Quantification of the types of keratin-filament organization observed in trophoblast giant cells derived from wild-type and *Mrj*$^{-/-}$ chorion-ectoplacental cone explants. (**C**) Ultrastructure of a keratin aggregate (surrounded by broken line) in a *Mrj*$^{-/-}$ trophoblast giant cell at E8.25. (**D**) Mrj expression (red) in trophoblast giant cells of a wild-type conceptus at E8.25. Right, higher-magnification of boxed region in the left panel. (**E**) Nuclear (left), cytoplasmic (center), and both nuclear and cytoplasmic (right) Mrj expression in wild-type trophoblast giant cells in vitro. Arrowheads indicate trophoblast giant cells with undetectable Mrj expression. Broken line indicates the periphery of a trophoblast giant cell. (A,D,E) DNA is blue. ch, chorion; em, embryo; pan-CK, pan-cytokeratin; TGC, trophoblast giant cells. Scale bars: 10 μm in A,E; 0.5 μm in C; 20 μm (left) and 10 μm (right) in D.

to show a phenotype. This suggests an alternative method of keratin regulation in *Mrj*-negative cells. Mrj was heterogeneously expressed in cultured trophoblast giant cells, either within the nucleus, the cytoplasm or both (Fig. 2E). This may be attributed to the presence of several trophoblast giant cell subtypes that appear both in vitro and in vivo (Simmons et al., 2007).

Keratin inclusion bodies disrupt the organization of *Mrj* mutant chorionic trophoblast

To investigate whether Mrj regulates the keratin cytoskeleton within the chorion, we analyzed K18 expression both in vitro and in vivo. In contrast to trophoblast giant cells, which showed heterogeneous expression, Mrj was uniformly expressed throughout the chorionic trophoblast layer (Fig. 3A). Trophoblast stem (TS) cell cultures are an established model for studying chorionic trophoblast cells in vitro (Tanaka et al., 1998; Uy et al., 2002). Therefore, we derived both wild-type and *Mrj*-deficient TS cell lines from littermate blastocysts generated from *Mrj* heterozygote crosses. Approximately 80% of wild-type TS cells (n=494) had normal K18 expression (Fig. 3B), whereas the remaining 20% had undetectable levels. By contrast, 78% of *Mrj*$^{-/-}$ TS cells (n=469) lacked a normal keratin network and contained keratin inclusions similar to, albeit smaller than, those seen within primary cultures of *Mrj*$^{-/-}$ trophoblast giant cells (Fig. 3C). K18 expression was less-apparent in histological sections of *Mrj*$^{-/-}$ chorionic trophoblast cells in vivo compared with wild type (Fig. 3E-H). However, electron microscopy confirmed the presence of filamentous aggregates (Fig. 3D). These data indicate that *Mrj* mutant chorionic trophoblast cells show the same type of keratin defects as trophoblast giant cells – both the lack of normal keratin cytoskeleton and the presence of large keratin aggregates – albeit at a higher frequency owing to the fact that a subset of giant cells do not express Mrj protein.

Next, we examined the ultrastructure of *Mrj*-deficient chorions to determine the effects of keratin aggregate formation on tissue integrity. In comparison to wild-type chorionic trophoblast cells (Fig. 3I,K), *Mrj*$^{-/-}$ cells were disorganized and rounded (Fig. 3J,L). This suggested that the adhesive properties of *Mrj*-null cells may have been altered. Therefore, we analyzed the expression of desmoplakin, a protein that links keratin filaments to desmosomes at the cell membrane. Remarkably, both *Mrj*$^{-/-}$ chorionic trophoblast cells and TS cells showed a significant reduction in desmoplakin immunofluorescence (Fig. 3O,P,R) compared with wild type (Fig. 3M,N,Q). Ultrastructurally, however, desmosomes appeared to be normal in *Mrj*$^{-/-}$ chorionic trophoblast cells (Fig. 3S,T). Together, these data imply that keratin inclusion bodies disrupt the organization of chorionic trophoblast cells, which in turn may affect the ability of the allantois to attach to the chorion. Notably, although they were disorganized, the *Mrj*$^{-/-}$ chorionic trophoblast cells showed no signs of cell death.

Proteasome degradation of keratin filaments requires Mrj

Keratin filaments can oligomerize without catalysts or co-factors (Owens and Lane, 2003; Quinlan et al., 1986). Accordingly, keratin inclusions both in *Mrj*-deficient chorionic trophoblast and in trophoblast giant cells contained filaments (Fig. 2C, Fig. 3D), indicating that Mrj was not necessary for filament assembly. Therefore, we reasoned that Mrj may have played a structural role or have been required for keratin turnover. We found that Mrj protein did not co-localize with K18-containing filaments in trophoblast giant cells (Fig. 4), implying that Mrj was not playing a direct role in the organization of the keratin filamentous network.

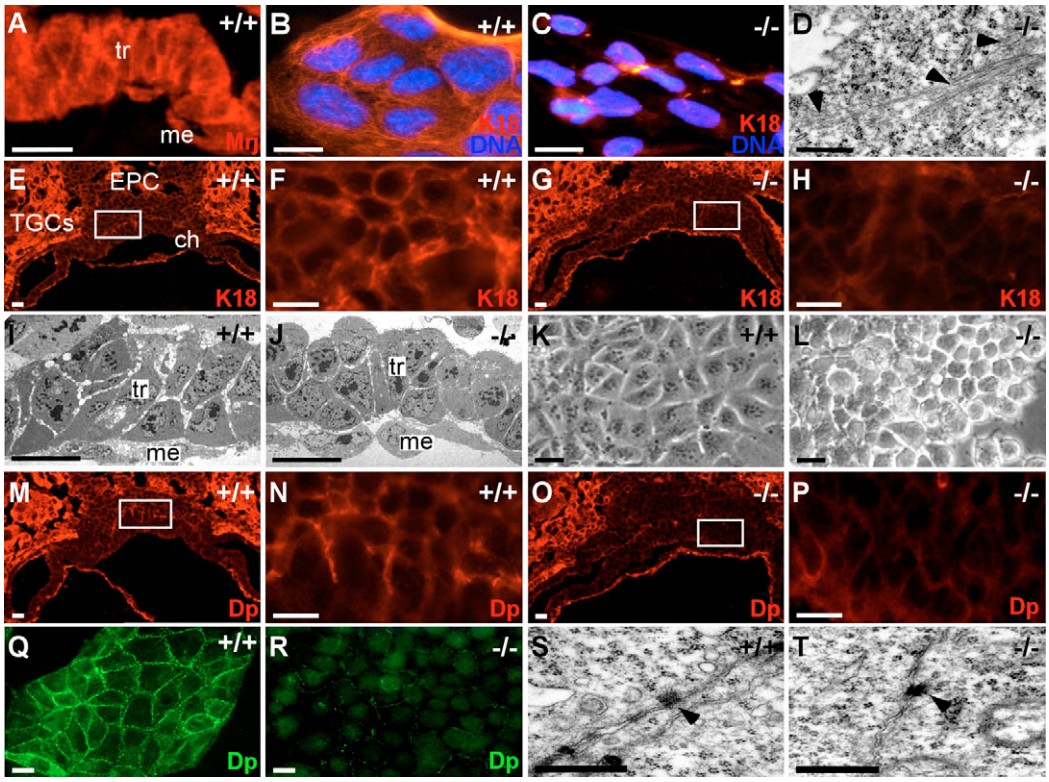

Fig. 3. Keratin inclusion bodies disrupt cell-cell adhesion and disrupt the organization of *Mrj*-deficient chorionic trophoblast cells. (**A**) Mrj expression (red) in a wild-type chorion at E8.25. (**B**,**C**) K18 expression (red) in wild-type (B; +/+) and *Mrj*-deficient (C; –/–) trophoblast stem (TS) cells. DNA is blue. (**D**) Ultrastructure of a keratin inclusion body (arrowheads) within a $Mrj^{-/-}$ chorionic trophoblast cell at E8.25. (**E-H**) K18 expression (red) in wild-type (E,F) and $Mrj^{-/-}$ (G,H) chorionic trophoblast cells at E8.25. (F,H) Higher-magnifications of boxed regions in E and G, respectively. (**I-L**) Morphology of *Mrj* mutant chorionic trophoblast cells in vivo (J) and in vitro (L) in contrast to wild-type cells (I,K). (**M-P**) Desmoplakin (Dp) expression (red) in wild-type (M,N) and $Mrj^{-/-}$ (O,P) chorionic trophoblast cells at E8.25. (N,P) Higher-magnifications of boxed regions in M and O, respectively. (**Q**,**R**) Desmoplakin expression (green) in wild-type (Q) and $Mrj^{-/-}$ (R) TS cells. (**S**,**T**) Electron micrographs of desmosomes (arrowheads) in wild-type (S) and $Mrj^{-/-}$ (T) chorionic trophoblast cells at E8.25. ch, chorion; DP, desmoplakin; EPC, ectoplacental cone; me, chorionic mesothelium; TGCs, trophoblast giant cells; tr, chorionic trophoblast. Scale bars: 10 μm in A-C,E-R; 0.5 μm in D,S,T.

It was previously shown that Mrj can interact with the soluble forms of K8/K18 (Izawa et al., 2000). Therefore, we next questioned whether Mrj regulated keratin by modulating the activity of the proteasome. Immunofluorescence of Mrj and 20S proteasome core subunits revealed that these two proteins co-localized (Fig. 5A). We then inhibited the proteasome complex in wild-type trophoblast giant cells by adding lactacystin (10 μM) and found that proteasome-inhibited cells contained large, perinuclear keratin inclusions (Fig. 5B) similar to $Mrj^{-/-}$ cells (Fig. 2A, Fig. 3C). Interestingly, Mrj co-localized with keratin inclusions within proteasome-inhibited cells (Fig. 5C). These data suggest that, without Mrj, keratin filaments are not properly degraded by the proteasome, leading to filament accumulation.

A minority of $Mrj^{-/-}$ conceptuses have hemorrhages reminiscent of keratin deficiency

Along with the formation of keratin aggregates, $Mrj^{-/-}$ trophoblast cells also lacked a properly organized keratin cytoskeleton. Previous studies have shown that an absence of the epithelial keratin cytoskeleton results in hemorrhaging within the trophoblast giant cell layer due to a loss of trophoblast cell integrity (Hesse et al., 2000; Jaquemar et al., 2003; Tamai et al., 2000). Interestingly, only 6.8% of *Mrj*-deficient embryos (4/59) developed placental site hemorrhages (see Fig. S2 in the supplementary material). No hemorrhages were observed in wild-type or heterozygous conceptuses (0/147). The rarity of placental hemorrhage in *Mrj* mutants indicated that the consequences of *Mrj* deficiency differ from those of keratin deficiency.

Keratin inclusion bodies are toxic to chorionic trophoblast cells and disrupt normal function

To investigate further whether keratin deficiency was responsible for the placental phenotype in $Mrj^{-/-}$ embryos, we assessed the occurrence of chorioallantoic attachment in keratin mutant mice. Chorioallantoic attachment was normal in both $K18^{-/-}$- and $K19^{-/-}$-knockout embryos (Fig. 6B,C and data not shown), resulting in mice that are viable and fertile (Hesse et al., 2000; Magin et al., 1998; Tamai et al., 2000). Although $K18^{-/-}$;$K19^{-/-}$ embryos have placental hemorrhages (Hesse et al., 2000), they all exhibited chorioallantoic attachment (n=8 double mutants from five litters) (Fig. 6D), indicating that this process can occur in the absence of a keratin cytoskeleton. This raised the possibility that keratin aggregation causes the *Mrj* phenotype. To address this, $Mrj^{+/-}$;$K18^{+/-}$ mice were mated and the resulting progeny (n=9 litters) were assessed for the presence of placental hemorrhages and chorioallantoic attachment. The incidence of placental hemorrhage in *Mrj* mutants was unaltered in $Mrj^{-/-}$;$K18^{+/-}$ (1/13) or $Mrj^{-/-}$;$K18^{-/-}$ (1/9) conceptuses. By contrast, 77% of $Mrj^{-/-}$;$K18^{+/-}$ embryos (10/13) and 100% of $Mrj^{-/-}$;$K18^{-/-}$ embryos (9/9) exhibited

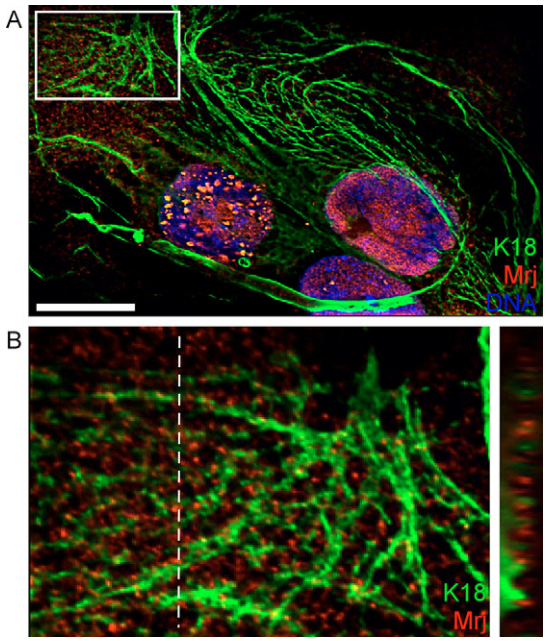

Fig. 4. Mrj protein expression does not co-localize to K18-containing filaments. (**A**,**B**) Deconvolved images of a trophoblast giant cell immunostained for Mrj (red), K18 (green) and DNA (blue). (B) Higher-magnification of the boxed region in A. A cross-section (broken line) appears on the far right side of B. Scale bar: 10 μm in A.

rescue of chorioallantoic attachment (Fig. 6E,F; Table 1). Histological analysis of rescued *Mrj*$^{-/-}$;*K18*$^{+/-}$ and *Mrj*$^{-/-}$;*K18*$^{-/-}$ placentas at E9.5 confirmed that chorioallantoic attachment had occurred and that subsequent villous formation was initiated. However, the chorionic plates remained compact with little branching or fetal blood vessel growth (Fig. 6H,I). Furthermore, fewer branchpoints were seen in *Mrj*$^{-/-}$;*K18*$^{+/-}$ chorionic plates (Fig. 6H) compared with those of *Mrj*$^{-/-}$;*K18*$^{-/-}$ (Fig. 6I). This contrasted with wild-type and *Mrj*$^{+/-}$;*K18*$^{+/+}$ littermate placentas (data not shown and Fig. 6G, respectively), which had extensive branching and vascularization within the labyrinth layers of their placentas.

Notably, *Mrj* and *K18* mutant mouse strains were maintained on different genetic backgrounds (CD-1 and 129Sv, respectively). However, *Mrj*$^{-/-}$ conceptuses in both CD-1 and 129Sv backgrounds fail to undergo chorioallantoic attachment (Hunter et al., 1999), indicating that the 129Sv genetic background, itself, is not sufficient to rescue chorioallantoic attachment in *Mrj*$^{-/-}$;*K18*$^{+/-}$ or *Mrj*$^{-/-}$;*K18*$^{-/-}$ embryos. Together, these results suggest that, by reducing the amount of keratin expressed, and thus aggregated, chorionic trophoblast cell function was restored and chorioallantoic attachment was rescued.

DISCUSSION

It is well-known that protein aggregation is associated with several degenerative diseases. We have shown here that both *Mrj*-deficient trophoblast giant cells and chorionic trophoblast cells lack a normal keratin cytoskeleton and contain large keratin inclusion bodies. Furthermore, we have implicated Mrj in the regulation of keratin-filament degradation. The inclusions resulting from *Mrj* deficiency are cytotoxic and prevent chorioallantoic attachment during placental development by affecting cell function but not viability.

Cells containing keratin inclusions, such as Mallory bodies, also have a diminished keratin cytoskeleton (Denk et al., 2000). To date, this has complicated our understanding of the consequences of protein aggregation. In this study, we have shown directly that keratin deficiency and keratin inclusion bodies have different effects. In the developing placenta, complete deficiency of the keratin cytoskeleton (e.g. *K8* mutants or *K18/19* double mutants) is associated with normal chorioallantoic attachment, whereas keratin inclusions (e.g. *Mrj* mutants) are associated with a failure in chorioallantoic attachment.

An essential function of keratin is to protect the cell against mechanical stresses (Owens and Lane, 2003). Mice that lack *K8* (Jaquemar et al., 2003), both *K8* and *K19* (Tamai et al., 2000) or both *K18* and *K19* (Hesse et al., 2000) fail to form keratin filaments in simple epithelial cells, such as trophoblast cells. As a result, mutant embryos die at approximately E10.5 because of compromised trophoblast cell integrity, which leads to placental site hemorrhages that are particularly associated with trophoblast giant cells. Despite a compromised keratin cytoskeleton in *Mrj* mutants, placental hemorrhage was rare, indicating that *Mrj* deficiency is distinct from

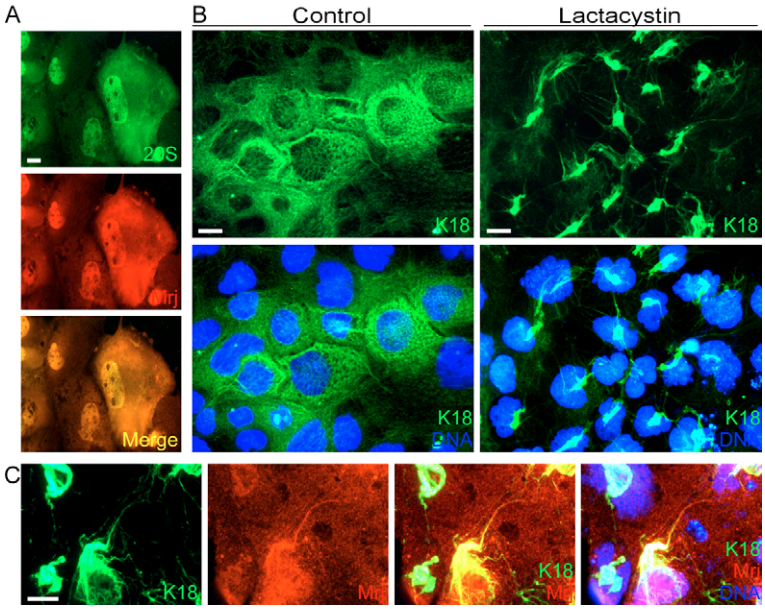

Fig. 5. Mrj is required for proteasome degradation of keratin filaments. (**A**) Expression of Mrj (red) and 20S proteasome core subunits (green) in wild-type trophoblast giant cells in vitro. (**B**) K18 expression (green) in trophoblast giant cells cultured with (right) or without (left) the proteasome inhibitor clasto-lactacystin β-lactone. (**C**) Mrj expression (red) in trophoblast giant cells treated with clasto-lactacystin β-lactone. K18 is green. (B,C) DNA is blue. Scale bars: 10 μm.

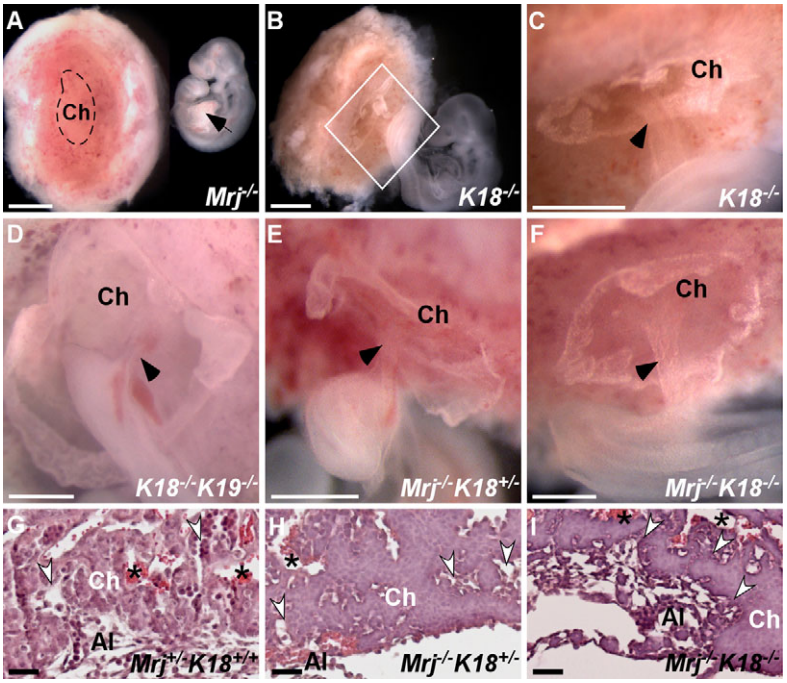

Fig. 6. Chorioallantoic attachment is rescued in *Mrj*$^{-/-}$;*K18*$^{+/-}$ and *Mrj*$^{-/-}$;*K18*$^{-/-}$ conceptuses. (**A**) An unattached allantois (arrow) of an E9.5 *Mrj*$^{-/-}$ embryo appears as a bud at the posterior end of the embryo. Broken line outlines the chorion (Ch). (**B-D**) Chorioallantoic attachment of *K18*$^{-/-}$ (B,C) and *K18*$^{-/-}$;*K19*$^{-/-}$ (D) conceptuses at E9.5. (C) Higher-magnification of the boxed region in B. (**E**,**F**) Rescued chorioallantoic attachment in *Mrj*$^{-/-}$;*K18*$^{+/-}$ (E) and *Mrj*$^{-/-}$;*K18*$^{-/-}$ (F) conceptuses at E9.5. (**G-I**) Branching morphogenesis in *Mrj*$^{-/-}$;*K18*$^{+/-}$ (H) and *Mrj*$^{-/-}$;*K18*$^{-/-}$ (I) placentas with rescued chorioallantoic attachment at E9.5 compared to a *Mrj*$^{+/-}$;*K18*$^{+/+}$ littermate placenta (G). White arrowheads, fetal blood space/branchpoint; asterisks, maternal blood space; Ch, chorion; Al, allantois; black arrowhead, allantois. Scale bars: 1 mm in A,B; 0.5 mm in C,D; 0.5 mm in E,F; 20 μm in G-I.

keratin deficiency. One explanation for this is that Mrj is not expressed in all trophoblast giant cells and, therefore, not all *Mrj*-deficient trophoblast giant cells lack a normal cytoskeleton or contain aggregates. This implies the involvement of another co-chaperone in the regulation of keratin degradation within these cells. As a result, trophoblast giant cells with a normal keratin cytoskeleton are probably interspersed with affected cells. This arrangement may be sufficient to maintain the integrity of the trophoblast giant cell layer surrounding the implantation site, preventing hemorrhage.

Intermediate filaments support a cell by attaching to desmosomes, cell-cell adhesion junctions at the cell membrane. Desmoplakin is not only required to attach filaments to the desmosome but it also maintains desmosomal stability (Gallicano et al., 1998). Desmoplakin mutants die at E6.5 because unstable desmosomes lead to a loss of integrity within extra-embryonic tissues (Gallicano et al., 2001; Gallicano et al., 1998). Normal localization of desmoplakin at the desmosome within *K18*$^{-/-}$;*K19*$^{-/-}$ trophoblast cells (Hesse et al., 2000) suggests that, in the absence of keratin filaments, desmosomes remain relatively stable. By contrast, *Mrj*-deficient chorionic trophoblast cells showed a significant reduction of desmoplakin expression. As a result, desmosomes in *Mrj*$^{-/-}$ trophoblast cells may be unstable, resulting in disrupted chorionic organization. This implies further that keratin inclusion bodies disrupt cell function independently of keratin deficiency. Presumably, the reduction of *K18* expression in *Mrj*$^{-/-}$;*K18*$^{+/-}$ and *Mrj*$^{-/-}$;*K18*$^{-/-}$ conceptuses decreased the amount of keratin aggregated, which in turn salvaged chorionic organization and rescued chorioallantoic attachment.

During chorioallantoic attachment, the allantois attaches directly to the chorionic mesothelium (Downs, 2002). However, there are a handful of genes, including *Mrj*, that are expressed only in the chorionic trophoblast and which, when knocked-out, result in chorioallantoic attachment defects (Hildebrand and Soriano, 2002; Parr et al., 2001; Saxton et al., 2001; Tetzlaff et al., 2004). This reveals that the mesothelium must interact with the trophoblast compartment for it to become receptive to the allantois. Conceptuses deficient for *Wnt7b*, a gene encoding a signaling protein secreted by chorionic trophoblast cells, fail to express α4-integrin (encoded for by *Itga4*), a mesothelially expressed adhesion molecule required for allantoic attachment (Parr et al., 2001; Yang et al., 1995). Interestingly, *Wnt7b*$^{-/-}$ chorions are disorganized (Parr et al., 2001), a phenotype reminiscent of *Mrj* deficiency. Although it was

Table 1. Incidence of chorioallantoic attachment in E9.5 embryos from intercrosses of *Mrj*$^{+/-}$;*K18*$^{+/-}$ mice

Genotype	Observed embryos with chorioallantoic attachment (%)*	Observed genotypic proportions (%)†	Expected genotypic proportions (%)†
Mrj$^{+/+}$;*K18*$^{+/+}$	100 (5/5)	6.2	6.25
Mrj$^{+/+}$;*K18*$^{+/-}$	100 (8/8)	9.9	12.5
Mrj$^{+/+}$;*K18*$^{-/-}$	100 (6/6)	7.4	6.25
Mrj$^{+/-}$;*K18*$^{+/+}$	100 (14/14)	17.3	12.5
Mrj$^{+/-}$;*K18*$^{+/-}$	100 (18/18)	22.2	25.0
Mrj$^{+/-}$;*K18*$^{-/-}$	100 (6/6)	7.4	12.5
Mrj$^{-/-}$;*K18*$^{+/+}$	0 (0/2)	2.5	6.25
Mrj$^{-/-}$;*K18*$^{+/-}$	77 (10/13)	16.0	12.5
Mrj$^{-/-}$;*K18*$^{-/-}$	100 (9/9)	11.1	6.25

*Total number of embryos=81.
†Total=100%.

previously shown that α4-integrin is expressed in *Mrj*$^{-/-}$ chorionic mesothelium (Hunter et al., 1999), it is unknown whether it is properly presented and active at the cell surface. Regardless, there are probably other unidentified adhesion mechanisms that are required because the chorioallantoic attachment phenotype in α4-integrin-deficient embryos is incompletely penetrant (Yang et al., 1995). This suggests that the disorganization of the *Mrj*$^{-/-}$ chorionic trophoblast layer may disrupt signaling between the trophoblast and mesothelium. Without this interaction, the mesothelium may not be prepared to receive the allantois, resulting in a failure of chorioallantoic attachment.

Molecular chaperones are components of the protein-folding machinery and can also be transformed into protein-degradation factors when bound to the correct regulatory proteins (Esser et al., 2004). The DnaJ co-chaperones not only regulate the ATPase activity and substrate-binding specificity of Hsp70, but also play a significant role in determining which chaperone pathway Hsp70 should pursue (Esser et al., 2004). For example, binding of Ydj1, a yeast homolog of DnaJ, to Hsp70 promotes the proper folding of its substrate (Meacham et al., 1999). By contrast, a human DnaJ homolog, HSJ1 (also known as DNAJB2 – Human Gene Nomenclature Database), and HSP70 stimulate substrate-ubiquitination and -sorting to the proteasome for degradation (Westhoff et al., 2005). MRJ can bind and activate HSP70 (Chuang et al., 2002; Izawa et al., 2000) yet, until now, determining whether this complex is involved in protein-folding or -degradation had never been pursued.

A limited number of chaperones interact with intermediate filaments, giving us few clues about how chaperone complexes regulate the keratin cytoskeleton (Izawa et al., 2000; Liao et al., 1995; Liao et al., 1997; Perng et al., 1999). The keratin network is highly dynamic, but surprisingly little is known about its regulation (Coulombe and Omary, 2002). A simple keratin filament, composed of heterodimers of type I (K18 or K19) and type II (K7 or K8) keratins, can form spontaneously without catalysts (Owens and Lane, 2003; Quinlan et al., 1986). Hsp70 (Izawa et al., 2000; Liao et al., 1995) and Mrj (Izawa et al., 2000) can associate with both soluble and filamentous forms of K8/K18. However, our finding that keratin filaments do form, albeit ending up in aggregates, within *Mrj*$^{-/-}$ trophoblast cells indicates that Mrj is not required for either keratin folding or keratin-filament assembly.

With the help of various proteins, keratin filaments bundle together and attach to desmosomes at the cell membrane to become organized into a dense network (Coulombe and Omary, 2002; Owens and Lane, 2003). We have shown here that Mrj is diffusely expressed throughout the cytoplasm, but does not localize onto K18-containing filaments in trophoblast cells. This suggests that Mrj is not involved in playing a structural role, which contradicts previous findings that described Mrj expression as filamentous (Izawa et al., 2000). This difference may be explained by the use of different cell types or by the resolution of imaging.

Keratin filaments can be remodeled or degraded by varying the levels of phosphorylation and ubiquitination (Coulombe and Omary, 2002; Ku and Omary, 2000). Our study demonstrates the involvement of Mrj in keratin degradation. As indicated above, Mrj does not co-localize to K18-containing filaments. However, it was previously demonstrated that Mrj can interact with the soluble fraction of K8/K18 proteins (Izawa et al., 2000). Furthermore, keratin inclusions in *Mrj*$^{-/-}$ cells are ultrastructurally similar to Mallory bodies that appear in the hepatocytes of patients with chronic liver disorders (Denk et al., 2000). A defect in the degradation mechanism of the proteasome is one cause of Mallory body formation because cells treated with inhibitors of proteasome function (Bardag-Gorce et al., 2004) or cells that contain the UBB^{+1} ubiquitin mutation (Bardag-Gorce et al., 2003) accumulate K18 and K8. We have shown here that Mrj protein co-localizes to the proteasome in trophoblast giant cells. When we chemically inhibited proteasome function in these cells, keratin aggregates formed that were similar to those in *Mrj*-deficient cells, suggesting that, in the absence of Mrj, K18 is not targeted to and/or degraded by the proteasome.

Mrj deficiency was associated with effects on the entire keratin cytoskeleton, such that K8-, K18- and K19-containing filaments aggregated. Previously, Mrj was shown to specifically interact with K18 but not with K8 (Izawa et al., 2000); however, whether Mrj associates with K19 is unknown. Because K18 and K19 are both type I keratins, it is plausible that Mrj also directly regulates K19-filament degradation. Alternatively, what may start as a primary effect on K18 protein aggregation may indirectly impair the activity of the ubiquitin-proteasome system, causing a vicious circle of protein aggregation (Bence et al., 2001; Esser et al., 2004). Another hypothesis suggests that there is interdependence between K8/K18 and K8/K19 filaments such that, if one type of filament aggregates, the other collapses into the inclusion body as well.

Our study clearly supports the hypothesis that the formation of keratin inclusion bodies in *Mrj*-deficient trophoblast cells is detrimental to cellular function rather than protective. If non-degraded keratin is sequestered to protect the cell, we would expect that the chorioallantoic attachment defect observed in *Mrj*$^{-/-}$ conceptuses is due to a non-functioning keratin cytoskeleton. However, *K18*$^{-/-}$;*K19*$^{-/-}$ embryos underwent chorioallantoic attachment. Instead, by genetically reducing or eliminating *K18* expression in *Mrj*-deficient embryos (*Mrj*$^{-/-}$;*K18*$^{+/-}$ or *Mrj*$^{-/-}$;*K18*$^{-/-}$), and thus reducing the amount of keratin aggregated, we observed that chorionic trophoblast cell function was restored and chorioallantoic attachment was rescued. This suggests that the keratin inclusions themselves are toxic to cells. Although we have not documented when keratin aggregates first appear in the trophoblast giant cells of *Mrj* mutants, it is remarkable that implantation occurs and that post-implantation development progresses as far as it does.

There are many mutants within the literature with defects in chorioallantoic attachment, yet several of these display incomplete penetrance (reviewed by Watson and Cross, 2005). Interestingly, mutant conceptuses that achieve chorioallantoic attachment will often exhibit later defects in morphogenesis of the labyrinth layer of the placenta (reviewed by Watson and Cross, 2005). Although chorioallantoic attachment was rescued in the majority of *Mrj*$^{-/-}$;*K18*$^{+/-}$ and *Mrj*$^{-/-}$;*K18*$^{-/-}$ placentas, the labyrinth layer remained under-developed such that little villous branching occurred within the chorionic plate and only a small amount of fetal vascularization was apparent. Furthermore, *Mrj*$^{-/-}$;*K18*$^{+/-}$ labyrinths were more-severely affected compared to those of *Mrj*$^{-/-}$;*K18*$^{-/-}$, suggesting that the continued presence of keratin aggregates, even at a reduced level, affects branchpoint morphogenesis and the subsequent development of the labyrinth. Reduced villous formation in *Mrj*$^{-/-}$;*K18*$^{-/-}$ placentas compared to wild type suggests that Mrj function may be required for labyrinth development independent of its role in keratin turnover. This implies that Mrj probably interacts with another substrate during this stage in placental development.

Mrj deficiency may affect a variety of tissues that express keratins, apart from the placenta, because *Mrj* is widely expressed both during later embryonic development and in the adult (Chuang et al., 2002; Hunter et al., 1999; Seki et al., 1999). In addition, Mrj has been shown to interact with other substrates (Chuang et al., 2002; Dai et al., 2005), notably the HD protein (Chuang et al., 2002). In Huntington's disease, mutant HD proteins with expanded N-terminal

repeats aggregate within neurons (DiFiglia et al., 1997). In vitro, the Mrj-Hsp70 complex can reduce the accumulation of mutant HD aggregates (Chuang et al., 2002). These data are consistent with a general role for Mrj in preventing intracellular inclusion bodies, probably by promoting protein degradation through the proteasome.

We gratefully acknowledge T. Magin for the K18 and K19 knockout mice and K19 antibody; M. Inagaki for the Mrj antibody; and J. Rossant for the Rs26 TS cell line. We also thank T. M. Magin, C. Schuurmans, D. R. Natale, D. G. Simmons, M. Hesse and the Cross laboratory members for critical scientific discussions. This work was supported by a grant from the Canadian Institutes of Health Research (CIHR) (to J.C.C.). E.D.W. was supported by a Queen Elizabeth II Graduate Scholarship and a studentship from the CIHR Training Program in Genetics: Child Health and Development. J.C.C. is an Investigator of the CIHR and a Scientist of the Alberta Heritage Foundation of Medical Research.

Supplementary material

Supplementary material for this article is available at
http://dev.biologists.org/cgi/content/full/134/9/1809/DC1

References

Bardag-Gorce, F., Riley, N., Nguyen, V., Montgomery, R. O., French, B. A., Li, J., van Leeuwen, F. W., Lungo, W., McPhaul, L. W. and French, S. W. (2003). The mechanism of cytokeratin aggresome formation: the role of mutant ubiquitin (UBB+1). *Exp. Mol. Pathol.* **74**, 160-167.

Bardag-Gorce, F., Vu, J., Nan, L., Riley, N., Li, J. and French, S. W. (2004). Proteasome inhibition induces cytokeratin accumulation in vivo. *Exp. Mol. Pathol.* **76**, 83-89.

Bence, N. F., Sampat, R. M. and Kopito, R. R. (2001). Impairment of the ubiquitin-proteasome system by protein aggregation. *Science* **292**, 1552-1555.

Carrell, R. W. (2005). Cell toxicity and conformational disease. *Trends Cell Biol.* **15**, 574-580.

Chuang, J. Z., Zhou, H., Zhu, M., Li, S. H., Li, X. J. and Sung, C. H. (2002). Characterization of a brain-enriched chaperone, MRJ, that inhibits Huntingtin aggregation and toxicity independently. *J. Biol. Chem.* **277**, 19831-19838.

Coulombe, P. A. and Omary, M. B. (2002). 'Hard' and 'soft' principles defining the structure, function and regulation of keratin intermediate filaments. *Curr. Opin. Cell Biol.* **14**, 110-122.

Dai, Y. S., Xu, J. and Molkentin, J. D. (2005). The DnaJ-related factor Mrj interacts with nuclear factor of activated T cells c3 and mediates transcriptional repression through class II histone deacetylase recruitment. *Mol. Cell. Biol.* **25**, 9936-9948.

Denk, H., Stumptner, C. and Zatloukal, K. (2000). Mallory bodies revisited. *J. Hepatol.* **32**, 689-702.

DiFiglia, M., Sapp, E., Chase, K. O., Davies, S. W., Bates, G. P., Vonsattel, J. P. and Aronin, N. (1997). Aggregation of huntingtin in neuronal intranuclear inclusions and dystrophic neurites in brain. *Science* **277**, 1990-1993.

Downs, K. M. (2002). Early placental ontogeny in the mouse. *Placenta* **23**, 116-131.

Esser, C., Alberti, S. and Hohfeld, J. (2004). Cooperation of molecular chaperones with the ubiquitin/proteasome system. *Biochim. Biophys. Acta* **1695**, 171-188.

Fan, C. Y., Lee, S. and Cyr, D. M. (2003). Mechanisms for regulation of Hsp70 function by Hsp40. *Cell Stress Chaperones* **8**, 309-316.

Gallicano, G. I., Kouklis, P., Bauer, C., Yin, M., Vasioukhin, V., Degenstein, L. and Fuchs, E. (1998). Desmoplakin is required early in development for assembly of desmosomes and cytoskeletal linkage. *J. Cell Biol.* **143**, 2009-2022.

Gallicano, G. I., Bauer, C. and Fuchs, E. (2001). Rescuing desmoplakin function in extra-embryonic ectoderm reveals the importance of this protein in embryonic heart, neuroepithelium, skin and vasculature. *Development* **128**, 929-941.

Hadjantonakis, A. K., Gertsenstein, M., Ikawa, M., Okabe, M. and Nagy, A. (1998). Generating green fluorescent mice by germline transmission of green fluorescent ES cells. *Mech. Dev.* **76**, 79-90.

Hartl, F. U. and Hayer-Hartl, M. (2002). Molecular chaperones in the cytosol: from nascent chain to folded protein. *Science* **295**, 1852-1858.

Hesse, M., Franz, T., Tamai, Y., Taketo, M. M. and Magin, T. M. (2000). Targeted deletion of keratins 18 and 19 leads to trophoblast fragility and early embryonic lethality. *EMBO J.* **19**, 5060-5070.

Hildebrand, J. D. and Soriano, P. (2002). Overlapping and unique roles for C-terminal binding protein 1 (CtBP1) and CtBP2 during mouse development. *Mol. Cell. Biol.* **22**, 5296-5307.

Hohfeld, J., Cyr, D. M. and Patterson, C. (2001). From the cradle to the grave: molecular chaperones that may choose between folding and degradation. *EMBO Rep.* **2**, 885-890.

Hunter, P. J., Swanson, B. J., Haendel, M. A., Lyons, G. E. and Cross, J. C. (1999). Mrj encodes a DnaJ-related co-chaperone that is essential for murine placental development. *Development* **126**, 1247-1258.

Izawa, I., Nishizawa, M., Ohtakara, K., Ohtsuka, K., Inada, H. and Inagaki, M. (2000). Identification of Mrj, a DnaJ/Hsp40 family protein, as a keratin 8/18 filament regulatory protein. *J. Biol. Chem.* **275**, 34521-34527.

Jaquemar, D., Kupriyanov, S., Wankell, M., Avis, J., Benirschke, K., Baribault, H. and Oshima, R. G. (2003). Keratin 8 protection of placental barrier function. *J. Cell Biol.* **161**, 749-756.

Ku, N. O. and Omary, M. B. (2000). Keratins turn over by ubiquitination in a phosphorylation-modulated fashion. *J. Cell Biol.* **149**, 547-552.

Liao, J., Lowthert, L. A., Ghori, N. and Omary, M. B. (1995). The 70-kDa heat shock proteins associate with glandular intermediate filaments in an ATP-dependent manner. *J. Biol. Chem.* **270**, 915-922.

Liao, J., Price, D. and Omary, M. B. (1997). Association of glucose-regulated protein (grp78) with human keratin 8. *FEBS Lett.* **417**, 316-320.

Lu, H., Hesse, M., Peters, B. and Magin, T. M. (2005). Type II keratins precede type I keratins during early embryonic development. *Eur. J. Cell Biol.* **84**, 709-718.

Magin, T. M., Schroder, R., Leitgeb, S., Wanninger, F., Zatloukal, K., Grund, C. and Melton, D. W. (1998). Lessons from keratin 18 knockout mice: formation of novel keratin filaments, secondary loss of keratin 7 and accumulation of liver-specific keratin 8-positive aggregates. *J. Cell Biol.* **140**, 1441-1451.

McClellan, A. J., Tam, S., Kaganovich, D. and Frydman, J. (2005). Protein quality control: chaperones culling corrupt conformations. *Nat. Cell Biol.* **7**, 736-741.

Meacham, G. C., Browne, B. L., Zhang, W., Kellermayer, R., Bedwell, D. M. and Cyr, D. M. (1999). Mutations in the yeast Hsp40 chaperone protein Ydj1 cause defects in Axl1 biogenesis and pro-a-factor processing. *J. Biol. Chem.* **274**, 34396-34402.

Nagy, A., Gertsenstein, M., Vintersten, K. and Behringer, R. (2003). Assembling aggregates between diploid and tetraploid embryos. In *Manipulating the Mouse Embryo: A laboratory Manual*. Vol. 1, pp. 496-497. Cold Spring Harbor, NY: Cold Spring Harbor Laboratory Press.

Owens, D. W. and Lane, E. B. (2003). The quest for the function of simple epithelial keratins. *BioEssays* **25**, 748-758.

Parr, B. A., Cornish, V. A., Cybulsky, M. I. and McMahon, A. P. (2001). Wnt7b regulates placental development in mice. *Dev. Biol.* **237**, 324-332.

Perng, M. D., Cairns, L., van den IJssel, P., Prescott, A., Hutcheson, A. M. and Quinlan, R. A. (1999). Intermediate filament interactions can be altered by HSP27 and alphaB-crystallin. *J. Cell Sci.* **112**, 2099-2112.

Quinlan, R. A., Hatzfeld, M., Franke, W. W., Lustig, A., Schulthess, T. and Engel, J. (1986). Characterization of dimer subunits of intermediate filament proteins. *J. Mol. Biol.* **192**, 337-349.

Rossant, J. and Cross, J. C. (2001). Placental development: lessons from mouse mutants. *Nat. Rev. Genet.* **2**, 538-548.

Saxton, T. M., Cheng, A. M., Ong, S. H., Lu, Y., Sakai, R., Cross, J. C. and Pawson, T. (2001). Gene dosage-dependent functions for phosphotyrosine-Grb2 signaling during mammalian tissue morphogenesis. *Curr. Biol.* **11**, 662-670.

Seki, N., Hattori, A., Hayashi, A., Kozuma, S., Miyajima, N. and Saito, T. (1999). Cloning, tissue expression, and chromosomal assignment of human MRJ gene for a member of the DNAJ protein family. *J. Hum. Genet.* **44**, 185-189.

Simmons, D. G. and Cross, J. C. (2005). Determinants of trophoblast lineage and cell subtype specification in the mouse placenta. *Dev. Biol.* **284**, 12-24.

Simmons, D. G., Fortier, A. L. and Cross, J. C. (2007). Diverse subtypes and developmental origins of trophoblast giant cells in the mouse placenta. *Dev. Biol.* doi:10.1016/j.ydbio.2007.01.009.

Tamai, Y., Ishikawa, T., Bosl, M. R., Mori, M., Nozaki, M., Baribault, H., Oshima, R. G. and Taketo, M. M. (2000). Cytokeratins 8 and 19 in the mouse placental development. *J. Cell Biol.* **151**, 563-572.

Tanaka, S., Kunath, T., Hadjantonakis, A. K., Nagy, A. and Rossant, J. (1998). Promotion of trophoblast stem cell proliferation by FGF4. *Science* **282**, 2072-2075.

Tarkowski, A. K., Witkowska, A. and Opas, J. (1977). Development of cytochalasin in B-induced tetraploid and diploid/tetraploid mosaic mouse embryos. *J. Embryol. Exp. Morphol.* **41**, 47-64.

Tetzlaff, M. T., Bai, C., Finegold, M., Wilson, J., Harper, J. W., Mahon, K. A. and Elledge, S. J. (2004). Cyclin F disruption compromises placental development and affects normal cell cycle execution. *Mol. Cell. Biol.* **24**, 2487-2498.

Uy, G. D., Downs, K. M. and Gardner, R. L. (2002). Inhibition of trophoblast stem cell potential in chorionic ectoderm coincides with occlusion of the ectoplacental cavity in the mouse. *Development* **129**, 3913-3924.

Watson, E. D. and Cross, J. C. (2005). Development of structures and transport functions in the mouse placenta. *Physiology Bethesda* **20**, 180-193.

Westhoff, B., Chapple, J. P., van der Spuy, J., Hohfeld, J. and Cheetham, M. E. (2005). HSJ1 is a neuronal shuttling factor for the sorting of chaperone clients to the proteasome. *Curr. Biol.* **15**, 1058-1064.

Yang, J. T., Rayburn, H. and Hynes, R. O. (1995). Cell adhesion events mediated by alpha 4 integrins are essential in placental and cardiac development. *Development* **121**, 549-560.